PNAS RESEARCH ARTICLE | APPLIED PHYSICAL SCIENCES

Osmotic and phoretic competition explains chemotaxic assembly and sorting

Aditya V. Hardikar[a,1,2], Adam W. Hauser[a,b,1,2], Terrence M. Hopkins[b], Stefano Sacanna[b], and Paul M. Chaikin[a]

Edited by Monica Olvera de la Cruz, Northwestern University, Evanston, IL; received June 3, 2024; accepted October 10, 2024

Microscale objects responding to chemical gradients by migrating toward or away from a preferred species is a simple yet constitutive mechanism by which transport occurs in biological organisms. Synthetic chemotaxis provides key physical descriptions of simplified systems that can be used in biological models, or in the creation of advanced responsive material systems. In this article, we provide a quantitative framework for understanding synthetic chemotaxis of microparticles which involves a competition between phoresis and osmosis. We present separate quantitative measurements of phoresis and osmosis acting on individual taxing particles, finding that phoresis follows the long-predicted $v \sim 1/r^2$ scaling while the osmotic contribution depends on the geometry and details of the system, and must be solved on a case-by-case basis. Through this, we are able to develop a more accurate picture of particle transport at the single particle level. Equipped with this approach, we go on to describe how high concentrations of particles in a symmetric chemical gradient grow close-packed hives that reach a steady-state size tunable through light intensity or particle size. Last, we demonstrate that mixed particles experiencing the same chemical gradient will selectively migrate toward or away depending on the nature of the particle surface, thereby locally sorting out a particular species. We anticipate these results will be important in describing both biological and synthetic chemotaxis in phoretic systems and should bring a wealth of studies that take advantage of competing osmotic flows to illicit unexpected dynamic active behavior.

chemotaxis | active matter | diffusiophoresis | soft matter | nonequilibrium assembly

Significance

Active synthetic matter has produced a wealth of exciting behavior from self-driven motile particles to flocking to phase separation. While there is no shortage of diverse experimental results from similar systems, how one determines the overall behavior for a given situation remains an open question. Long understood to be present, but often dismissed, the osmotic component in phoretic chemotaxis can play an important role. We quantitatively separate osmosis from phoresis and provide a general pathway to approach analysis near surfaces. One can use this to describe behaviors such as finite-sized hive formation and particle sorting. Through this approach, we expect old systems can be understood and additional unique behaviors identified with implications from advanced materials to biology.

Chemotaxis drives a myriad of transport processes within biological organisms. Particularly interesting examples include leukocytes that can sense chemicals released by bacteria and migrate toward an infection (1), tropism in flowers that make pollen tubes grow in the direction of the ovary (2), and bear deterrent sprays that effectively repel bears away from specific chemicals (3). Synthetic systems involving self-taxing particles and combinations of chemically active and taxable particles have attracted great attention over the past decade due to the exciting nonequilibrium and dynamic assemblies created therefrom (4–12). For such active matter at the micron scale, phoresis and osmosis are two well-known mechanisms for driving chemotaxis. We can subcategorize transport driven by gradients such as chemical, thermal, or electric potential, as chemo-, thermo- and electrophoresis (13–17). All these nonequilibrium phoretic effects arise from interactions between fluid components and the particle interface such that the particle motion can be calculated by considering fluid dynamics in an interfacial region near the particle (14, 18–22). Despite being studied for over a century, phoretic and osmotic phenomena are not well understood, difficult to predict, and even have conflicting experimental observations (23–27). Although it has long been known that these chemophoretic effects find a counterpart in chemo-osmosis (i.e., migration of fluid in response to a chemical gradient from a fixed surface), there is a lack of detailed theory and experiment that considers the overall effect on a taxing particle. Recent studies have pointed to the importance of osmosis (5, 28), but in most cases it is assumed that phoresis dominates and the resulting phoretic models achieve qualitative agreement with experiments at best (4, 29). In the present study, we work to separate these effects, use this knowledge to model and control nonequilibrium steady-state assemblies, and show that mixtures of particles can be chemotaxically selected for such assemblies.

Using a system of catalytic and polymer particles that are purely repulsive at equilibrium, we show that upon light-triggered chemical gradient formation, attractive velocities v dependent on distance r do not simply follow a $v \sim \nabla c \sim 1/r^2$; a relationship that arises from purely phoretic hydrodynamic models (14, 19, 20, 30) when considering a diffusive chemical concentration profile ($c \sim 1/r$). Instead, we find that the overall velocity $v(r)$ involves contributions from osmotic flow due to interaction

Author affiliations: [a]Center for Soft Matter Research, Department of Physics, New York University, New York, NY 10003; and [b]Department of Chemistry, New York University, New York, NY 10003

Author contributions: A.V.H., A.W.H., S.S., and P.M.C. designed research; A.V.H., A.W.H., and T.M.H. performed research; A.V.H., A.W.H., and T.M.H. analyzed data; and A.V.H., A.W.H., S.S., and P.M.C. wrote the paper.

The authors declare no competing interest.

This article is a PNAS Direct Submission.

[1]A.V.H. and A.W.H. contributed equally to this work.

[2]To whom correspondence may be addressed. Email: avh292@nyu.edu or adam.hauser@nyu.edu.

This article contains supporting information online at https://www.pnas.org/lookup/suppl/doi:10.1073/pnas.2410840121/-/DCSupplemental.

Published November 14, 2024.

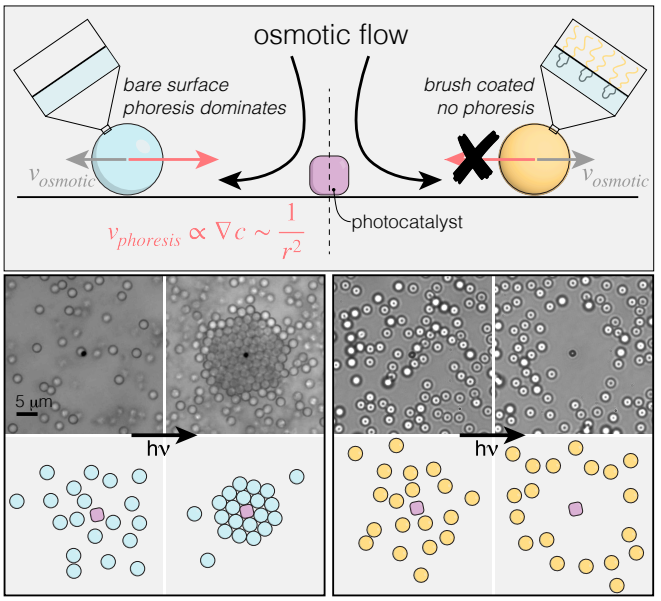

Fig. 1. Summary of chemotaxic behavior. Photocatalytic particles (purple cube) generate a chemical gradient that bare particles (blue) migrate toward since the phoretic velocity ($v \sim 1/r^2$) is greater than the osmotic velocity—the nature of which is shown in Fig. 2*B* and is nontrivial, depending on surface chemistry and system geometry. Brush coated particles (yellow) that do not experience phoresis migrate away due to this osmotic flow. When particle to catalyst ratios are high, bare particles grow close packed structures, while the brush coated particles form an exclusion zone.

of the chemical gradient with neighboring surfaces. This effect is nontrivial and depends on the neighboring surface chemistry and the geometry of the system, calculated only by solving for the complete hydrodynamics of the system. In the system presented, we find that the measured velocity v is a complex function of r, involving a phoresis part that goes as $v \sim 1/r^2$, and an osmotic part which does not have a closed form relationship with r. However, in our case, the velocity can be approximated by a power law $v(r) \sim \kappa/r^{\nu}$ over a short range from 2 to 10 μm, but differs based on the experimental parameters and system geometry. Experiments performed on a glass substrate result in a surface flow away from the catalyst. In the absence of phoretic effects, particles advect away from the catalyst approximately at the fluid velocity as dictated by Faxen's Law (31). Historically, this contribution was ignored, with experimental data fit to $v \sim 1/r^2$ (4, 29) as the overall behavior is generally dominated by phoresis.

Through experimental measurements of bare and polymer brush coated particles in the same chemical gradient, a more quantitative picture of chemotaxic transport of micro-objects is formed (Fig. 1), which necessitates a competition between phoresis pulling the particles inward and osmosis pushing them out. We go on to quantitatively describe and control steady-state crystalline assemblies created through these nonequilibrium forces and demonstrate that particle mixtures can be locally sorted by a chemical gradient.

Results and Discussion

Individual Chemotaxis. We consider a system of colloidal α-iron oxide (hematite) in a basic solution containing hydrogen peroxide that, upon blue light illumination, catalyzes the degradation of H_2O_2 into water and O_2 (4, 32, 33). Using continuity and flux conservation of the generated chemical species, the chemical concentration goes as $c(r) \sim 1/r$, where r is the distance from the center of the catalyst. According to hydrodynamic theory of chemophoresis (19, 20, 30), the velocity $v(r)$ of a spherical colloid in a linearly varying concentration gradient $c(r)$ goes as $v(r) \sim \nabla c(r)$ which implies that velocity scales as $1/r^2$. In basic solution, bare poly(3-(trimethoxysilyl)propylmethacrylate) (TPM), sulfate-initiated poly(styrene) (PS) or silica (SiO_2) colloids, move toward a higher chemical concentration near the catalyst and cluster around it to form a hexagonal lattice due to excluded volume effects (Fig. 1*B*). We note that it is quite probable that the causal chemical gradient is not simply dissolved O_2 or H_2O_2 and may well be dominated by charged intermediates or background ionic species as others have suggested (29, 34, 35). Here, we do not attempt to dispute this and treat the problem without chemical specificity but caution the reader that background chemical or concentration changes will likely affect both phoretic and osmotic components discussed throughout this article.

If the experiments are performed near a substrate, such as glass, that is attracted to higher concentrations of product (4, 5), a lateral osmotic slip velocity arises at the surface directed away from the catalyst due to interaction of the chemical species generated with the substrate that also scales as $v_{slip}(r) \sim 1/r^2$. This creates an advective flow that depends on the specific geometry of the system and recirculation of fluid. As the schematic in Fig. 1*A* suggests, if one is able to "turn off" phoresis, a nearby particle will follow this developed advective flow away from the catalyst. We are able to experimentally observe this with polymer brush coated particles (29, 36–39) that remove the phoretic effect (Fig. 2*A*) as will be discussed in more detail below.

Since the advective osmotic flow is present in both brush coated and bare particles, we aim to understand consequences of this competition and quantify the overall chemotaxic mobilities and resulting assembled structures. First, we examine the behavior of single particles interacting with a gradient. Catalyst colloids are fixed to the surface of rectangular cross-section glass capillaries which are subsequently filled with a low concentration of TPM colloids in basic H_2O_2 solution. Upon illumination and chemical gradient formation, the particle positions are tracked in time. The osmotic velocity component should not follow any particular function and will likely not have a closed form solution as it depends on the gradient chemistry, the nature of the particle and glass interfaces, and the exact geometry of the system. However, in this system, with r values ranging from 2 to 10 μm, a closed form solution is useful in examining hive formation later on. The resulting velocity $v(r)$ vs. center-to-center distance r gives a relationship that can be approximated by a power law $v(r) \sim \kappa/r^{\nu}$, where ν is 2.9 in Fig. 2 and κ is a fitting parameter. Indeed, when we change the particle size, we observe variation in ν and κ, as is discussed later and shown in Fig. 3*D*. This emphasizes that one must solve for the complete hydrodynamics of the system by considering the osmotic component of the chemotaxic velocity for any given system to fully utilize and understand the behavior.

To confirm and quantify the effect of the osmotic flow, we perform the experiments with the same TPM particles but with a neutral polymer brush on the surface to remove the phoretic contribution to the taxis. Fig. 2*A* (gray circles) shows the velocity relationship to r when particles are only being advected by the osmotic flow. Interestingly, we observe a crossover point at very close distances—below which the particles will have an attractive velocity and above they will be repelled.

To bolster these findings, we perform finite-element analysis simulations using the geometry of the experimental system. We impose a slip velocity on the bottom surface which takes the

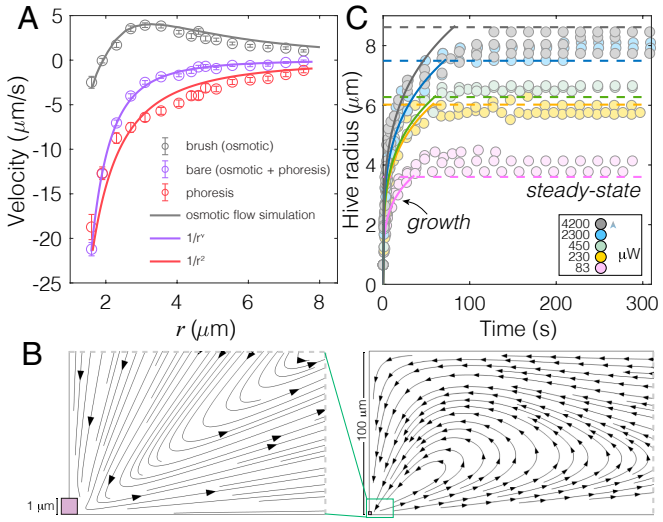

Fig. 2. Individual taxis and hive growth. (*A*) Single particle speeds measured from center-to-center distance r between particle and a spatially fixed catalyst of brush coated particles (gray circles) and bare particles (purple circles); purely phoretic contribution (red circles) are acquired by subtracting the gray from the purple points; the gray line is a result from finite-element simulations shown in (*B*); the purple line is a best fit to $1/r^{\nu}$ where ν is 2.9 in this case, and the red line is a best fit to $1/r^2$. (*B*) Flow lines from finite-element simulations of our system with a defined slip velocity at the lower boundary of $v = \alpha/r^2$ and no-slip conditions on all other surfaces; the solid line in (*A*) is found by taking the velocity at the height of the catalyst particle (1 μm); α is determined empirically through a best match of the experimental data. (*C*) Hive size in time at varying incident light intensity showing a clear growth and steady-state phase (circles); solid lines are calculated from the growth model and dashed lines are calculated from the steady-state model as described in the text.

form $v_{slip}(r) = \alpha \nabla c(r)$, where α is a constant obtained from experiments, while all other walls including the catalyst surface are assigned a no-slip condition. According to Faxen's law (31), the velocity of an advecting particle in a flow is equal to the value of the fluid velocity evaluated at the center of the particle in the undisturbed flow (i.e., when the particle is absent). The calculated advective velocity profile taken at a height of 1 μm above the surface (the center of the particle) matches the experimentally determined particle velocities remarkably well. We note that the real concentration profile of the chemical gradient will be affected by the generated fluid advection which will in turn modify the slip velocity condition. Our approximation that $c \sim 1/r$ is justified by the fast pace of molecular diffusion relative to advection. The time for an ion/molecule to diffuse over a distance d having a diffusivity D gives a timescale for diffusion $\tau_{diff} = \frac{d^2}{D}$, whereas advection is $\tau_{adv} = \frac{d}{v}$, where v is the velocity at d. Comparing at $d = 10$ μm, $v = 1$ μm/s and $D = 10^{-9}$ m^2/s, the ratio is $\frac{\tau_{diff}}{\tau_{adv}} = \frac{vd}{D} \sim \frac{10^{-11}}{10^{-9}}$, illustrating that advection can be safely neglected as the diffusion time is about two orders of magnitude smaller.

To isolate the phoretic portion of the bare particle chemotaxis, we simply subtract the brush coated velocities to recover the long predicted $v(r) \sim 1/r^2$ relationship as shown in Fig. 2*A*. The value of κ', extracted from the fit $v = \frac{\kappa'}{r^2}$ is 56.9±1.7 μm^3/s. Although the osmotic contribution to chemotaxic particle transport will vary per system, it is clear that it must be taken into account for a full understanding of mobility and resulting emergent assemblies.

Assembly. With a large excess of bare particles (10^5:1 particles:catalyst), we see growth of crystalline assemblies that ultimately reach a steady-state size which is tunable by light intensity (Fig. 2*C*). Using the knowledge of individual chemotaxic velocities described above, we can quantitatively describe these two stages of assembly. The chemical gradient produced by a catalyst particle attracts bare particles nearby resulting in the growth of a hive, analogous to processes in biology such as bacterial colony formation (40), accumulation of leukocytes at sites of infection in the human body (41) or honeybees balling predatory wasps as a defense mechanism (42). Moreover, these hives tend to be hexagonally close packed structures when the bare particles are uniformly sized.

To derive an analytical model for the hive growth stage (Fig. 3*A*), we use the experimentally acquired velocity vs. distance relationship with the approximated form $v(r) \sim \kappa/r^{\nu}$ as discussed previously. Additionally, we assume that the chemical gradient is instantaneously generated at t_0, which corresponds to the light being switched on. This is a valid assumption as the timescale for chemical diffusion and achieving a steady state is two orders of magnitude smaller than the timescale for a particle reaching the catalyst. At a later time t, particles that were within a distance ℓ at t_0 will become a part of the hive of size $R(t)$. A particle that starts out exactly at a distance ℓ at t_0, moving with a velocity $v(r)$, given by the expression above, reaches the hive at time t which has grown to a size R. Integrating the velocity expression with these boundary conditions ($r(t_0) = \ell$ and $r(t) = R$) gives the expression

$$\ell^{\nu} - R^{\nu} = (\nu + 1)\kappa(t - t_0). \quad [1]$$

A second relation can be obtained by particle conservation. Taking ρ_0 as the background areal concentration of particles in the plane of the catalyst at t_0, we can say that

$$\rho_0 \pi \ell^2 = \phi R^2/a^2, \quad [2]$$

where a is the particle radius and ϕ is the packing fraction. Substituting for ℓ in the previous relation gives us an expression for the hive growth in time. Again, using our velocity approximation, we get a closed form solution of the hive size with time, given by

$$R(t)^{\nu+1} = \frac{(\nu + 1)\kappa(t - t_0)}{\left(\frac{\phi}{\pi \rho_0 a^2}\right)^{(\nu+1)/2} - 1}, \quad [3]$$

where the constant κ and exponent ν is acquired from single particle velocity experiments like the purple curve in Fig. 2*A* and will vary with bulk conditions and particle size as demonstrated in Fig. 3*D*. Fig. 3*B* shows that the hive growth is well described by this model—closely following a best fit to three different hive growth curves.

At some point in time, a sharp size cut-off is observed that represents a steady-state (Fig. 2*C*). We explain this through balancing particle drift $v(r)$ toward the catalyst, as described above, against Brownian diffusion D_B. A particle diffusion current away from the edge of a hive arises from the concentration gradient surrounding a growing hive relative to the bulk concentration ρ_0. This outward flux balanced with the drift can be expressed as $D_B \frac{d\rho}{dr} = \rho v(r)$, which gives a steady-state profile of the form $\rho(r) = Ae^{\frac{1}{D_B}\int v(r)dr}$. Solving for a distance from the hive edge Δr, where the concentration falls by an order of magnitude gives $\Delta r = D_B/v(r)$. If $\Delta r = a$, the concentration falls by an order of magnitude over the length of a particle and the colloids are no longer tightly packed. This yields our expression for the steady-state hive size (R_{ss}) given by

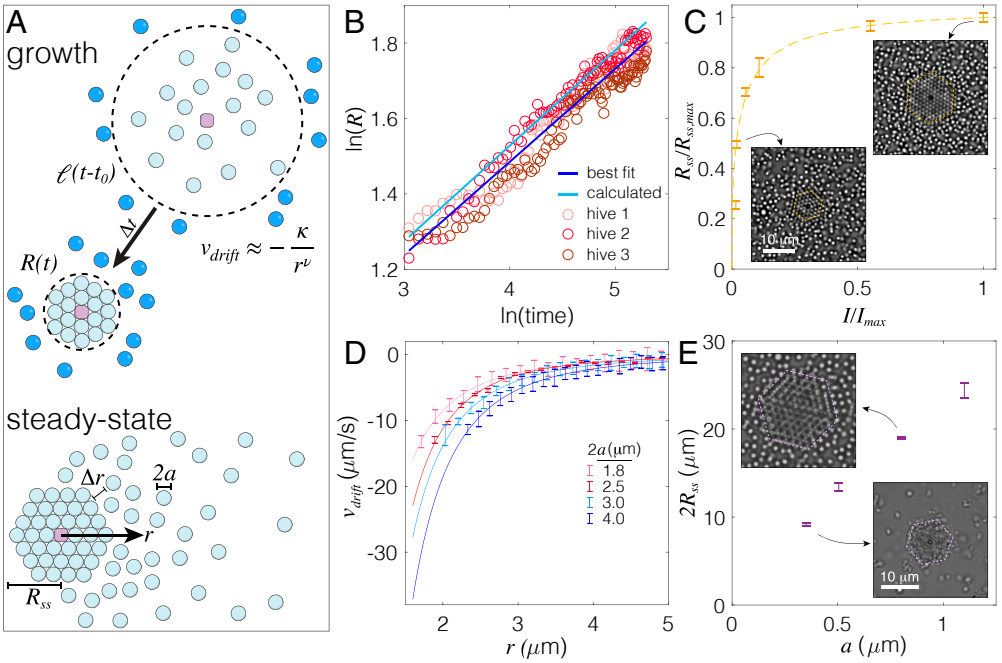

Fig. 3. Hive formation and analysis. (*A*) (*Top*) Growth model depicting the state of the system at two times—t_0 when the light is switched on and no hive has formed and a later time t when the hive grows to a size $R(t)$; (*Bottom*) steady-state hive showing a particle concentration decreasing with distance away from hive edge. (*B*) Hive size as a function of time during the growth phase; best fit line closely agrees with the calculated curve from the growth model (Eq. **3**). (*C*) Relative steady-state hive size as a function of relative light intensity growing as predicted by theory and fit with Eq. **5**. (*D*) Single particle velocity with center-to-center distance for four different particle sizes. (*E*) Steady-state hive size increases monotonically with particle size when all other variables are fixed.

$$R_{ss}^{\nu} = \kappa a / D_B, \qquad [4]$$

which corresponds to the last particle added to the hive having a Péclet number $Pe = va/D_B \sim 1$.

Armed with this description, we can move on to describe how to tune the hive size at steady state. Light intensity modulates the photocatalytic reaction rate, and thus can be used to tune the size. To quantify this effect, we limit the κ term in a Michaelis–Menten reaction–diffusion framework which takes the form $\kappa = \kappa_{max}\left(\frac{I}{I+\beta}\right)$, where β is a constant that limits κ to a κ_{max}. Invoking our expression for R_{ss}, we find that

$$\widetilde{R}_{ss} = \left((1+\varepsilon)\frac{\widetilde{I}}{\widetilde{I}+\varepsilon}\right)^{1/\nu}, \qquad [5]$$

where $\widetilde{R}_{ss}$ and $\widetilde{I}$ are the relative hive size and intensity, and ε is a constant. Fig. 3*C* shows this expression agrees very well with our data, showing that these formed structures are predictable and easily tunable with light intensity.

As the osmotic contribution to the overall drift velocity does not follow any particular scaling or function, to explore how particle size a affects the steady-state hive size one must first perform single particle experiments exemplified in Fig. 2*A* to obtain the relevant $v(r)$ for each a under otherwise identical conditions. We observe in Fig. 3*D* that our simplified form for the overall velocity still fits the data quite well, but κ varies from -59 to -160 and ν from 2.8 to 3.2. Strikingly, Fig. 3*D* shows an increasing velocity with particle size trend that appears to counter the generally accepted size-independent phoretic relationship. In fact, when we subtract osmotic contributions (*SI Appendix*, Fig. S4), the curves collapse, indicating that pure phoresis is indeed independent of particle size and that the osmotic contribution to the overall velocity becomes less important with increasing particle size (*SI Appendix*, Fig. S5) (13, 19). We can see that a monotonic increase in R_{ss} with particle size should occur according to Eq. **4**, thus particle size is another means to control steady-state hive size. It is instructive again to compare the Péclet numbers at a given r to quickly see that v and a increase and D_B decreases with particle size; therefore, more particles must be added to a hive before unity is achieved. We experimentally demonstrate this tunability in Fig. 3*E*.

Chemotaxic Sorting. Finally, as is commonplace in biology, we demonstrate that this chemical gradient can select and thus locally concentrate a particular species over another. In these experiments, silica and fluorescent TPM of similar sizes are mixed at a ratio of about 2:3 silica:TPM with the α-iron oxide catalyst, where the total particle:catalyst ratio is about 200:1. We perform experiments with bare and brush coated fluorescent TPM, but maintain all other variables constant. The silica particles are bare, negatively charged, and behave largely the same as a bare TPM particle—that is, they are drawn toward the chemical gradient produced by our catalyst particles due to phoretic dominance over osmotic flow.

A mixture of the bare TPM and silica shows that the catalyst collects the silica and bare TPM at nearly the same ratio as the background concentration as one would expect for a randomly distributed particle mixture (Fig. 4*A*). In contrast, when brush coated TPM and silica are mixed, the catalyst selects the silica particles almost exclusively, while the brush coated TPM are repelled by osmotic flow (Fig. 4*B*). The small number of particles that end up in the hive are either due to brush density variation, or they are in very close proximity to the catalyst before the light is turned on and are attractive according to our findings in Fig. 2*A*. The silica concentrations are enriched from 35% in the background to 98% in the hives on average—a 180% increase.

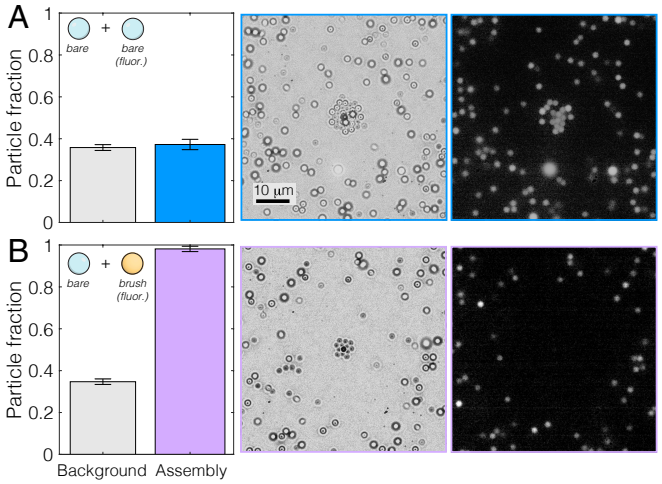

Fig. 4. Particle sorting. Hive formation from mixed particles where the histograms show the average background bare (SiO_2) particle fractions and the optical images show a representative brightfield and fluorescent image for the same hive; hive particle fractions are counted at 300 s after the light is turned on and represents ≥20 hives; total particle/catalyst ratio is about 200. (*A*) bare and bare fluorescent particle mixture; (*B*) bare and brush coated fluorescent particle mixture.

Conclusion

We have presented a quantitative view of synthetic chemotaxis near a substrate that illustrates the importance of opposing osmotic flow on the overall behavior of taxing particles. Through individual particle analysis, we show that particles can be either attractive or repulsive in the same gradient. At high particle concentrations, bare, attractive, particles are shown to grow close packed hexagonal crystals that ultimately reach a steady-state size. This is shown to be limited by the increasing importance of Brownian diffusion farther away from the catalyst center. The steady-state size can be tuned by light intensity and particle size. Last, we demonstrate that a chemical gradient can select and locally concentrate bare particles over brush coated particles with a rejection rate close to 100%. The results presented on individual particle motion have implications in many chemotaxic systems—both synthetic and biological—that occur near surfaces, while our hive growth model illustrates that nonequilibrium forces can give rise to tunable steady-state structures, which differs from any equilibrium system.

Materials and Methods

Materials. All chemicals were used as received unless otherwise noted. Sodium hydroxide, hydrogen peroxide (30%), ammonium hydroxide (30%), Pluronic F108, potassium persulfate (KPS, >99%), styrene (>99%), 2,2′-azobis(2-methylpropionitrile), and ferric chloride hexahydrate (ACS reagent, 97%) were purchased from Sigma Aldrich. 3-(trimethoxysilyl)propyl methacrylate (98%) was purchased from Gelest inc. Absolute ethanol was purchased from Fisher Sci. Silica particles were purchased from Spherotech Inc.

Methods.

α-iron oxide catalyst. Cube-shaped catalysts are synthesized following a well-known gel-sol method (32). Briefly, 5.4 M aqueous sodium hydroxide was slowly introduced into a 200 mL Pyrex bottle containing 2.0 M aqueous $FeCl_3$ hexahydrate solution under constant swirling by hand. The reaction forms a brown thick gel that is warm to the touch. The bottle is then capped and vigorously shaken for ten minutes before placing in an oven at 100 °C for eight days. During this process, the reaction mixture turns dark red, indicative of the complete conversion of gel to hematite cubes. The suspension is then washed via gravity sedimentation with deionized water four times before use.

Poly(TPM) synthesis. TPM colloids are synthesized by the well-known spontaneous emulsification process (43), followed by radical polymerization of the methacrylate moieties. The particle size is tuned by adjusting the concentration of 3-(trimethoxysilyl)propyl methacrylate and/or the NaOH concentration, while other parameters are held constant. An example procedure to obtain 2 μm diameter particles is as follows. In a 50 mL polypropylene centrifuge tube with a total reaction volume of 40 mL, deionized water, 3 mM NaOH, and 3 vol% 3-(trimethoxysilyl)propyl methacrylate are added before placing the tube on a rotator (IKA Loopster) at 10 RPM for 3 h. It is important to swiftly add the 3-(trimethoxysilyl)propyl methacrylate to the basic water in one portion with as little agitation as possible to prevent nucleation time variation and thus decreased size homogeneity, and begin the slow rotation as soon as possible after addition. When the reaction is complete, 10 mg of AIBN is added to the solution and gently stirred before allowing polymerization to take place at 70 °C for 6 h. The suspension is mixed gently to prevent significant sedimentation every 30 min for the first 2 h of the polymerization. The poly(3-(trimethoxysilyl)propyl methacrylate) is purified by centrifugation and resuspension in deionized water at least four times–diluting about 20× each time.

To make the brush coated TPM, the procedure is exactly as above before polymerization. After the spontaneous emulsification reaction, an aqueous solution of the amphiphilic triblock copolymer Pluronic F108 is added to reach 0.1 wt% in the solution (0.8 mL at 5 wt% in water) and allowed to incubate for 10 min before adding AIBN and heating. This procedure is done to ensure the PPO segments of the triblock copolymer are kinetically trapped in the methacrylate-siloxane network such that they can no longer desorb. The brush coated TPM are washed at least six times in the same manner as the uncoated TPM to remove as much free F108 polymer as possible.

Polystyrene synthesis. Polystyrene colloids are synthesized by known surfactant-free emulsion polymerization methods. As an example, to synthesize 800 nm diameter particles, seeded growth using 400 nm seed particles is employed. For the seeds, 500 mL of deionized water and 50 mL of styrene are added to a 1 L 3-neck round bottom flask. The mixture is brought to 60 °C, sparged with N_2 and stirred for 30 min before injecting 0.21 g KPS dissolved in 10 mL of deionized water. The mixture is allowed to stir at 330 RPM under N_2 overnight. The particles are washed with repeated centrifugation-resuspension cycles at 3,000 RPM for 4 h. For seeded growth, the same procedure is used with 500 mL deionized water, 55 mL styrene, and 12 mL seed particle suspension (2 wt%) is added to the flask before heating, sparging, and initiation. The resultant particles are washed repeatedly with centrifugation-resuspension cycles at 1500 RPM for 4 h.

Silica treatment. A 500 μL suspension of 5% v/v of silica microparticles is centrifuged, washed, and resuspended in DI water to a total volume of 500 μL three times. We place this in a plastic vial and puncture a few holes in the top of the vial with a syringe tip. We place this suspension in a bath at 70 °C and add in order 500 μL of 30% ammonium hydroxide NH_4OH followed by a 30% hydrogen peroxide H_2O_2 solution, similar to the procedure highlighted in Van Kesteren et al. (44). The particles are again washed repeatedly with DI water before use. This cleans the surface by removing organic contaminants from the surface of the microparticles.

COMSOL simulations. We used COMSOL multiphysics to model the osmotic flow field. In order to do this, we use the laminar flow module and replicate the geometry of the system, with a 1 μm hematite sitting at the base of a capillary 100 μm high. We use axial symmetry about an axis perpendicular to the base of the capillary and center of the hematite, effectively using a cylindrical hematite cube 1 μm wide sitting at the base of a cylindrical capillary 100 *upmu*m high and 1,000 μm long. We use the finest mesh size available. An osmotic slip velocity is imposed on the bottom surface equal to γ/r^2, where r is the distance from the center of the hematite cube. We later determine the value of the free parameter γ, by matching the osmotic advective velocity on a particle comparing it with experiments done with brush coated particles. This is done by selecting the value of γ that minimizes the least sum of squares error between the two curves–simulation and experiment.

Growth model. To derive the growth model, we ignore particle diffusion since the molecular Péclet number $Pe \ll 1$ and only consider the drift velocity of bare particles moving toward the catalyst given by

$$v = \frac{dr}{dt} \sim \frac{\kappa}{r^\nu}, \quad [6]$$

where the nonuniversal $v \sim \kappa/r^\nu$ dependence is a good fit to the measured behavior. Integrating the velocity expression with these boundary conditions ($r(t_0) = \ell$ and $r(t) = R$)

$$\int_\ell^R \frac{dr}{v(r)} = t - t_0, \quad [7]$$

which yields the equation for a single particle trajectory that starts at a distance ℓ at t_0 and reaches the edge of the hive of size R at time t, we get

$$\ell^\nu - R^\nu = (\nu + 1)\kappa(t - t_0). \quad [8]$$

Any particle starting at time t_0 within a distance ℓ will be a part of the hive at time t, and any particles further away than ℓ will not. This gives us a second relation that conserves the total number of particles starting within a distance ℓ at t_0 with initial concentration ρ_0 packing in the hive at time t given by

$$\pi\ell^2\rho_0 = \frac{\phi\pi R^2}{\pi a^2}, \quad [9]$$

where ϕ is the packing fraction of particles. Both these equations together give

$$R(t)^{\nu+1} = \frac{(\nu + 1)\kappa(t - t_0)}{(\frac{\phi}{\pi\rho_0 a^2})^{(\nu+1)/2} - 1}. \quad [10]$$

Steady-state model. Steady-state hive size is reached as a result of a competition between drift and diffusion. The flux due to drift bringing particles toward the catalyst is given by

$$J_{\text{drift}} = -\rho v(r) \sim -\rho\frac{\kappa}{r^\nu}, \quad [11]$$

where the drift velocity is approximated by a power law. The competing diffusive flux taking particles from a region of high concentration near the hive to low concentration far away is

$$J_{\text{diff}} = D_B\frac{d\rho}{dr}. \quad [12]$$

Equating J_{drift} and J_{diff}, which is the condition for steady state yields

$$\frac{d\rho}{\rho} = -\frac{\kappa}{D_B}\frac{dr}{r^\nu}. \quad [13]$$

Plugging in the boundary conditions where the background concentration is ρ_0 as $r \to \infty$, we obtain the steady state particle concentration outside the hive

$$\rho(r) = \rho_0 e^{\frac{\kappa}{D_B r^{\nu-1}}}. \quad [14]$$

Using this, the distance Δr at which the concentration falls by an order of magnitude is

$$\Delta r = \frac{D_B r^\nu}{\kappa}. \quad [15]$$

If this Δr is equal to the size of a particle a, we are no longer tightly packed in the hive and in steady state, giving us the steady state hive size R_{ss}

$$R_{\text{ss}}^\nu = f\frac{\kappa a}{D_B}, \quad [16]$$

where f is an arbitrary factor ($\sim$2.5 for particles used in the majority of the article) which depends on the size of particles, packing fraction, and how the size of hive is measured, factors not taken into account in this model.

Single particle tracking experiments. 1 μL of a 1% hemtatite colloid suspension is diluted with 99 μL ethanol. This is filled into glass capillaries and flash dried in the oven at 80 °C, which sticks the hematite to the glass. A dilute suspension of colloidal TPM ($<10^5$ particles/mL) at pH 12 (done by adding 10 mM NaOH) and 1% H_2O_2 as chemical fuel is filled into glass capillaries (VitroCom #5012-050) and sealed with wax. This capillary with a fixed hematite colloid and diffusing TPM particles is imaged with a Nikon Ti-E microscope. Light from a SOLA light engine is filtered using a bandpass filter (400 to 450 nm Thorlabs FESH0450) which provides blue light that illuminates the hematite. These particle trajectories are tracked and analyzed using the TrackPy library in Python (45) based on the Crocker-Grier algorithm (46), which yields the velocity vs. distance curves as presented

It is known that the background ionic strength and pH will affect the magnitude and sign of the velocity, and we do see such an effect in this system as others have studied (4, 29). The basic conditions are chosen additionally so that we can use a combination of uncoated glass, negatively charged particles, and polymer coated particles without any one species aggregating with or adsorbing to one another.

High particle/catalyst ratio experiments. For experiments that form colloidal hives, we use the same procedure to fix hematite cubes along with a high concentration of satellite colloids ($>10^8$ particles/mL), keeping the NaOH and peroxide concentration the same. When the colloids are illuminated with blue light, hive growth is tracked and the size is monitored using appropriate thresholding and locating the boundary.

Data, Materials, and Software Availability. All study data are included in the article and/or supporting information.

ACKNOWLEDGMENTS. We thank Shihao Zang and Sarah Chong for synthesizing the polystyrene particles used in this study. We thank Jeana Zheng and Steven van Kesteren for discussions regarding polymer brush grafting and surface treatment. We also thank John Brady and Alexander Grosberg for fruitful discussions regarding osmosis and phoresis. The research was primarily supported by Grant DOE DE-SC-0020976. We acknowledge support from DOE DE-SC0007991 for computation of hydrodynamic flows.

1. M. McCutcheon, Chemotaxis in leukocytes. *Physiol. Rev.* **26**, 319–336 (1946).
2. M. Welk, W. Millington, W. G. Rosen, Chemotropic activity and the pathway of the pollen tube in lily. *Am. J. Bot.* **52**, 774–781 (1965).
3. T. S. Smith, S. Herrero, T. D. Debruyn, J. M. Wilder, Efficacy of bear deterrent spray in Alaska. *J. Wildl. Manage.* **72**, 640–645 (2008).
4. J. Palacci, S. Sacanna, A. P. Steinberg, D. J. Pine, P. M. Chaikin, Living crystals of light-activated colloidal surfers. *Science* **339**, 936–940 (2013).
5. D. Boniface, S. G. Leyva, I. Pagonabarraga, P. Tierno, Hydrodynamics is needed to explain propulsion in chemophoretic colloidal rafts. arXiv [Preprint] (2023). https://arxiv.org/abs/2309.11084 (Accessed 18 January 2024).
6. J. Palacci, S. Sacanna, A. Vatchinsky, P. M. Chaikin, D. J. Pine, Photoactivated colloidal dockers for cargo transportation. *J. Am. Chem. Soc.* **135**, 15978–15981 (2013).
7. A. Aubret, M. Youssef, S. Sacanna, J. Palacci, Targeted assembly and synchronization of self-spinning microgears. *Nat. Phys.* **14**, 1114–1118 (2018).
8. W. Wang, W. Duan, A. Sen, T. E. Mallouk, Catalytically powered dynamic assembly of rod-shaped nanomotors and passive tracer particles. *Proc. Natl. Acad. Sci. U.S.A.* **110**, 17744–17749 (2013).
9. D. Feldmann *et al.*, Manipulation of small particles at solid liquid interface: Light driven diffusioosmosis. *Sci. Rep.* **6**, 36443 (2016).
10. M. C. Marchetti *et al.*, Hydrodynamics of soft active matter. *Rev. Mod. Phys.* **85**, 1143 (2013).
11. W. Wang, W. Duan, S. Ahmed, A. Sen, T. E. Mallouk, From one to many: Dynamic assembly and collective behavior of self-propelled colloidal motors. *Acc. Chem. Res.* **48**, 1938–1946 (2015).
12. W. F. Paxton *et al.*, Catalytic nanomotors: Autonomous movement of striped nanorods. *J. Am. Chem. Soc.* **126**, 13424–13431 (2004).
13. R. Piazza, A. Parola, Thermophoresis in colloidal suspensions. *J. Phys.: Condens. Matter* **20**, 153102 (2008).
14. H. Brenner, Phoresis in fluids. *Phys. Rev. E* **84**, 066317 (2011).
15. P. Rowghanian, A. Y. Grosberg, Electrophoresis of a DNA coil near a nanopore. *Phys. Rev. E* **87**, 042723 (2013).
16. J. T. Ault, S. Shin, H. A. Stone, Diffusiophoresis in narrow channel flows. *J. Fluid Mech.* **854**, 420–448 (2018).
17. M. Braibanti, D. Vigolo, R. Piazza, Does thermophoretic mobility depend on particle size? *Phys. Rev. Lett.* **100**, 108303 (2008).
18. J. L. Anderson, Colloid transport by interfacial forces. *Annu. Rev. Fluid Mech.* **21**, 61–99 (1989).
19. E. Ruckenstein, Can phoretic motions be treated as interfacial tension gradient driven phenomena? *J. Coll. Interface Sci.* **83**, 77–81 (1981).
20. R. Golestanian, Phoretic active matter. arXiv [Preprint] (2019). https://arxiv.org/abs/1909.03747 (Accessed 3 November 2023).

21. M. Von Smoluchowski, Elektrische endosmose und stromungsstrome. *Handb. Elektriz. Magn.* **2**, 366 (1921).
22. B. Derjaguin *et al*., Surface forces in transport phenomena. *Surf. Forces*, 369–431 (1987).
23. S. Duhr, D. Braun, Thermophoretic depletion follows Boltzmann distribution. *Phys. Rev. Lett.* **96**, 168301 (2006).
24. S. A. Putnam, D. G. Cahill, G. C. Wong, Temperature dependence of thermodiffusion in aqueous suspensions of charged nanoparticles. *Langmuir* **23**, 9221–9228 (2007).
25. C. Felix *et al*., Electrophoresis and stability of nano-colloids: History, theory and experimental examples. *Adv. Coll. Interface Sci.* **211**, 77–92 (2014).
26. S. Ebbens, M. H. Tu, J. R. Howse, R. Golestanian, Size dependence of the propulsion velocity for catalytic Janus-sphere swimmers. *Phys. Rev. E* **85**, 020401 (2012).
27. W. Volkmuth, R. Austin, DNA electrophoresis in microlithographic arrays. *Nature* **358**, 600–602 (1992).
28. D. Cao *et al*., A conceptual framework to understand the self-assembly of chemically active colloids. *Langmuir* **40**, 10884–10894 (2024).
29. X. Zhou *et al*., Ionic effects in ionic diffusiophoresis in chemically driven active colloids. *Phys. Rev. Lett.* **127**, 168001 (2021).
30. J. L. Anderson, D. C. Prieve, Diffusiophoresis: Migration of colloidal particles in gradients of solute concentration. *Sep. Purif. Methods* **13**, 67–103 (1984).
31. J. Happel, H. Brenner, *Low Reynolds Number Hydrodynamics: With Special Applications to Particulate Media* (Springer Science & Business Media, 2012), vol. 1.
32. T. Sugimoto, M. M. Khan, A. Muramatsu, Preparation of monodisperse peanut-type α-Fe_2O_3 particles from condensed ferric hydroxide gel. *Coll. Surf. A: Physicochem. Eng. Aspects* **70**, 167–169 (1993).
33. Y. Y. Avital *et al*., Two-site H_2O_2 photo-oxidation on haematite photoanodes. *Nat. Commun.* **9**, 4060 (2018).
34. A. M. Brooks *et al*., Shape-directed rotation of homogeneous micromotors via catalytic self-electrophoresis. *Nat. Commun.* **10**, 495 (2019).
35. A. Brown, W. Poon, Ionic effects in self-propelled Pt-coated Janus swimmers. *Soft Matter* **10**, 4016–4027 (2014).
36. A. Zheng, "DNA-coated colloids: Diffusion and electrokinetic characterization," Dissertation, New York University, New York, NY (2023).
37. R. J. Hill, D. Saville, W. Russel, Electrophoresis of spherical polymer-coated colloidal particles. *J. Coll. Interface Sci.* **258**, 56–74 (2003).
38. J. Harden, D. Long, A. Ajdari, Influence of end-grafted polyelectrolytes on electro-osmosis along charged surfaces. *Langmuir* **17**, 705–715 (2001).
39. M. Youssef, A. Morin, A. Aubret, S. Sacanna, J. Palacci, Rapid characterization of neutral polymer brush with a conventional zetameter and a variable pinch of salt. *Soft Matter* **16**, 4274–4282 (2020).
40. C. A. Weber, Y. T. Lin, N. Biais, V. Zaburdaev, Formation and dissolution of bacterial colonies. *Phys. Rev. E* **92**, 032704 (2015).
41. M. Baggiolini, Chemokines and leukocyte traffic. *Nature* **392**, 565–568 (1998).
42. T. Ken *et al*., Heat-balling wasps by honeybees. *Naturwissenschaften* **92**, 492–495 (2005).
43. C. Van Der Wel *et al*., Preparation of colloidal organosilica spheres through spontaneous emulsification. *Langmuir* **33**, 8174–8180 (2017).
44. S. van Kesteren, X. Shen, M. Aldeghi, L. Isa, Printing on particles: Combining two-photon nanolithography and capillary assembly to fabricate multimaterial microstructures. *Adv. Mater.* **35**, 2207101 (2023).
45. D. B. Allan, T. Caswell, N. C. Keim, C. M. van der Wel, R. W. Verweij, soft-matter/trackpy: Trackpy v0. 5.0. Zenodo repository (2021). https://soft-matter.github.io/trackpy/dev/. Accessed 27 May 2023.
46. J. C. Crocker, D. G. Grier, Methods of digital video microscopy for colloidal studies. *J. Coll. Interface Sci.* **179**, 298–310 (1996).